Electrostriction and guidance of acoustic phonons in optical fibers

Jean-Charles Beugnot and Vincent Laude[*]

Institut FEMTO-ST, Université de Franche-Comté and CNRS, Besançon, France

We investigate the generation of acoustic phonons in optical fibers via electrostriction from coherent optical waves. Solving the elastodynamic equation subject to the electrostrictive force, we are able to reproduce the experimental spectra found in standard and photonic crystal fibers. We discuss the two important practical cases of forward interaction, dominated by elastic resonances of the fiber, and backward interaction, for which an efficient mechanism of phonon guidance is found. The last result describes the formation of the coherent phonon beam involved in stimulated Brillouin scattering.

PACS number(s): 42.65.Es, 63.20.D−, 77.65.−j, 78.20.hb

Electrostriction (ES) describes the coherent generation of acoustic phonons from the interference of two frequency-detuned optical waves. The effect is closely related to Brillouin light scattering (BLS), or the scattering of an incident photon by an acoustic phonon of a solid material, accompanied by a frequency shift of the scattered photon. The combination of BLS and ES explains stimulated Brillouin scattering (SBS), an efficient three-wave interaction involving two optical waves and an acoustic wave satisfying both energy and momentum conservation. SBS is a fundamental limiting phenomenon for signal transport over optical fibers.[1] Interactions of photons and acoustic resonances of photonic crystal fibers (PCF)[2] and optical waveguides[3] have received much attention, for instance, in view of obtaining strong opto-acoustic interactions[4] or of reducing noise in quantum optics experiments.[5] ES in optical fibers is not easily observed since, while the incident and the scattered optical waves are directly accessible to the experiment, the intervening acoustic phonons are only witnessed via their induced effects on light. As a result, most theories eliminate phonon dynamics to concentrate on the evolution of the amplitudes of optical waves. This process, however, can only be performed under strong assumptions on the nature of the phonons generated by ES. Guided acoustic wave Brillouin scattering (GAWBS) theories, for instance, assume the acoustic modal shapes and resonant frequencies to be known beforehand, so that scattering cross sections can be computed from overlap integrals.[6–8] Modal approaches, however, give no insight into the mechanism of selection of particular phonons from the electrostrictive force.

In this paper, we propose a direct calculation of acoustic phonons induced by electrostriction in optical fibers, based only on knowledge of the fiber geometry and of the particular incident guided optical waves. Specifically, an elastodynamic equation is solved for a fiber with an arbitrary cross section subject to an optical force. By comparing with the experimental spectra obtained with the standard optical fiber and photonic crystal fiber with a solid core, we show that the computed phonons as a function of the detuning frequency explain both backward and forward ES and provide an estimation of the efficiency of the process. Under the phase-matching conditions of SBS, furthermore, our results imply that the phonon beam generated by electrostriction is actually guided and confined to the core of the fiber.

Standard SBS models for optical fibers are based on a rather strong plane-wave approximation[9,10] and on the picture of ES-generated pressure or density fluctuation waves.[1] In contrast to this simple picture, theory and experiment have shown the relevance of including both shear and longitudinal elastic waves together with a precise description of the structure.[2,6,7,11] Let us consider an optical fiber with an arbitrary cross section. We assume the total incident optical field results from the superposition of two frequency-detuned guided modes

$$E(r,z;t) = E^{(1)}(r)e^{i(\omega_1 t - k_1 z)} + E^{(2)}(r)e^{i(\omega_2 t - k_2 z)}, \quad (1)$$

with angular frequencies $\omega_{1(2)}$ and axial wave vectors $k_{1(2)}$. This optical distribution induces an optical force given by divergence of the symmetric ES stress tensor $T_{ij}^{es} = -\epsilon_0 \chi_{klij} E_k E_l^*$, with the rank-4 susceptibility tensor $\chi_{klij} = \varepsilon_{km}\varepsilon_{ln}p_{mnij}$ and p_{mnij} the elasto-optic tensor. ϵ_0 is the permitivity of a vacuum. The force term with detuning frequency $\omega = \omega_1 - \omega_2$ is proportional to $E_k^{(1)} E_l^{(2)*} \exp[i(\omega t - kz)]$ with $k = k_1 - k_2$. Because we are considering the generation of elastic waves with low frequency with respect to optical frequencies $\omega \ll \omega_{1,2}$. If the two optical waves are propagating in the same direction, a situation typical of GAWBS,[6] $k \approx 0$ and we speak of forward ES. If they are propagating in opposite directions, which is the SBS situation, $k \approx 2k_1$ and we speak of backward ES. Because of the particular source term, the following ansatz is assumed for the displacements of the ES-generated elastic wave

$$u_i(r,z;t) = \bar{u}_i(r)e^{i(\omega t - kz)}, \quad (2)$$

where the transverse dependence $\bar{u}_i(r)$ is the unknown of the model. The elastodynamic equation

$$\rho \frac{\partial^2 u_i}{\partial t^2} - (c_{ijkl}u_{k,l})_{,j} = -T_{ij,j}^{es}, \quad (3)$$

with c_{ijkl} the rank-4 tensor of elastic constants, is written in variational form by left-multiplying by virtual displacement field v_i and integrating over the cross section S. Further applying Green's theorem, we get

$$-\omega^2 \int_S \rho v_i^* u_i + \int_S v_{i,j}^* c_{ijkl} u_{k,l} = \int_S dr v_{i,j}^* T_{ij}^{es}, \quad (4)$$

which amounts to the theorem of virtual work for the ES force. For practical computations, the Galerkin nodal finite element method (FEM) is then employed to transform the

integral equation into the linear system

$$[K(k) - \omega^2 M]U = X(k)T^{es}, \tag{5}$$

with mass matrix M, stiffness matrix $K(k) = K_0 + kK_1 + k^2K_2$, and $X(k) = X_0 + kX_1$. U is the vector of nodal displacements $\bar{u}_i$ and T^{es} is the vector of electrostriction stress tensor value at nodal points $\bar{T}^{es}_{ij} = -\epsilon_0 \chi_{klij} E_k^{(1)} E_l^{(2)*}$. Equation (5) is our central result. Its solution as a function of frequency detuning gives the rigorous distribution of displacements within the waveguide cross section and can be directly compared to experiment, as we show next. The ES stress tensor is uniquely defined by the optical modal distribution. Matrices $K(k)$ and $X(k)$ are polynomials in the wave-vector detuning k, thus unifying in the same formula forward and backward ES, as well as any intermediate situation.

As a test for our model, we selected a 1-km long single mode fiber (SMF28) and a 400-m long large core PCF with similar optical propagation properties. Single mode guidance is achieved by total internal reflection: SMF28 has a Ge-doped core with a larger refractive index than the surrounding undoped silica, while PCF has a pure-silica core surrounded by a holey structure with a lower effective index. The silica PCF shown as an inset in Fig. 2(a) has a hole diameter of 4.6 μm and an air filling ratio $d/\Lambda = 0.58$, resulting for the fundamental mode in effective index $n_{eff} = 1.441$ and optical effective area $A_{eff} = 70$ μm^2. The SMF28 fiber has $n_{eff} = 1.446$ and $A_{eff} = 78.3$ μm^2, while the core diameter is 8.2 μm.

ES-generated phonons inside an optical fiber are hardly observable directly. They can, however, be observed indirectly in a manner similar to spontaneous Brillouin gain spectrum measurement or Brillouin sensing, by monitoring the light diffracted from a coherent pump wave. A heterodyne detection experimental setup was used for investigating backward ES.[12] To observe forward ES, we used a fiber loop mirror interferometer.[8] The measured spectra for the SMF28 fiber are shown in Figs. 1(a) and 1(b). The forward spectrum has many sharp peaks that gradually vanish for frequencies above 600 MHz. The peaks are known to be directly related to elastic resonances of the fiber. The backward spectrum shows a single Lorentzian peak with a linewidth of 27 MHz and a central frequency 10.85 GHz. The PCF case shown in Figs. 2(a) and 2(b) looks similar, though the resonance frequencies are slightly different. Forward ES resonances in this case are known to be related to the holey structure rather than to the external cladding of the fiber.

We then proceed to model the experimental results using Eq. (5). A FEM mesh covering the full fiber cross section was first created, with the outer boundaries left free. The mesh of the PCF was extracted from the scanning electron microscope image shown as an inset in Fig. 2(a). The fundamental optical modes are first obtained and normalized for unit transported power. ES stress distributions are displayed in Figs. 1(c) and 2(c). For both fibers, the ES stress is confined in the core roughly as the square of the optical field. Next, the ES-driven elastodynamic equation was solved for the displacement of the elastic wave by imposing the phonon wave vector k and scanning the detuning frequency ω. Independent material constants considered for silica are shown in Table I. To include

the phonon lifetime, elastic losses were incorporated in the ES model by considering a complex elastic tensor whose imaginary part is a constant viscosity tensor times frequency.[13] This loss model is compatible with the usual assumption that the Qf product is a constant for a given material, with Q the quality factor and f the frequency. This is the only adjustable parameter in the model. The value $Qf = 5.10^{12}$ Hz was selected to fit the SBS linewidth of SMF28.

Calculated forward ($k = 0$) and backward ($k = 2k_1$) ES spectra are shown in Figs. 1(a) and 2(a) for SMF28 and PCF, respectively. These spectra are obtained by evaluating the kinetic energy in the phonon beam $\omega^2/2 \int_S \rho |u_i|^2$ as a function of frequency detuning. The agreement with the experimental spectra is excellent in the backward case, with only one Lorentzian peak appearing. In the forward case, the appearance of a sequence of sharp resonance peaks and its gradual disappearance with increasing frequency are correctly reproduced, though the relative peak heights are not accurately predicted. These discrepancies can be explained by fine details of the fiber away from the core that are not described precisely in the model, while they can have a direct influence on transverse phonon resonances. Such discrepancies were already noted by Shelby *et al.*,[6] when comparing modal theory with the experiments.

We display in Figs. 1(d) and 2(d) the kinetic energy densities at resonance for selected frequencies in the forward ES spectrum. For SMF28, the energy distribution fills the whole fiber. For PCF, in contrast, the phonons are confined by the holey microstructure. For both fibers, the maximum displacement is of the order of 150 fm and is dominantly transversal. The situation is dramatically different in the backward case since the phonon beam is found to be confined to the core for both fibers. For both fibers, the maximum displacement is of the order of 50 fm and is dominantly longitudinal, though transversal displacements do not vanish.

Let us discuss the above results in light of the elastic normal modes of the fiber section. Such an approach has been successful to describe GAWBS in classical fibers[16] and recently in PCF.[2,8,17,18] It has also been used to describe the phononic crystal properties of PCF.[7,11] For a given wave vector k, the modes are obtained in the absence of any applied force as solutions of the eigenvalue problem $KU = \omega^2 MU$. Because the fiber cross section has finite dimensions, the spectrum of eigenmodes ω_n is discrete. Modes are such that their potential and kinetic energy are equal $U_n^\dagger KU_n = \omega_n^2 U_n^\dagger MU_n$. They are furthermore orthogonal, or $U_m^\dagger KU_n = U_m^\dagger MU_n = 0$, provided $\omega_m \neq \omega_n$. They thus constitute a complete basis, and the solution to the forced equation can be expanded as

$$U = \sum_n \frac{\omega_n^2}{\omega_n^2 - \omega^2} \frac{U_n^\dagger X T^{(es)}}{U_n^\dagger KU_n} U_n. \tag{6}$$

As a consequence, the phonon response to the electrostrictive excitation is a sequence of Lorentzian-shaped resonances; at each resonance frequency, the modal shape is a normal mode of the fiber. Clearly, the electrostriction gain is governed by the overlap integral $U_n^\dagger X T^{(es)} = \int_V dr (u_n)_{i,j}^* T_{ij}^{es}$, that compares the strain field of each mode with the electrostrictive stress distribution. Because of elastic losses, the response cannot
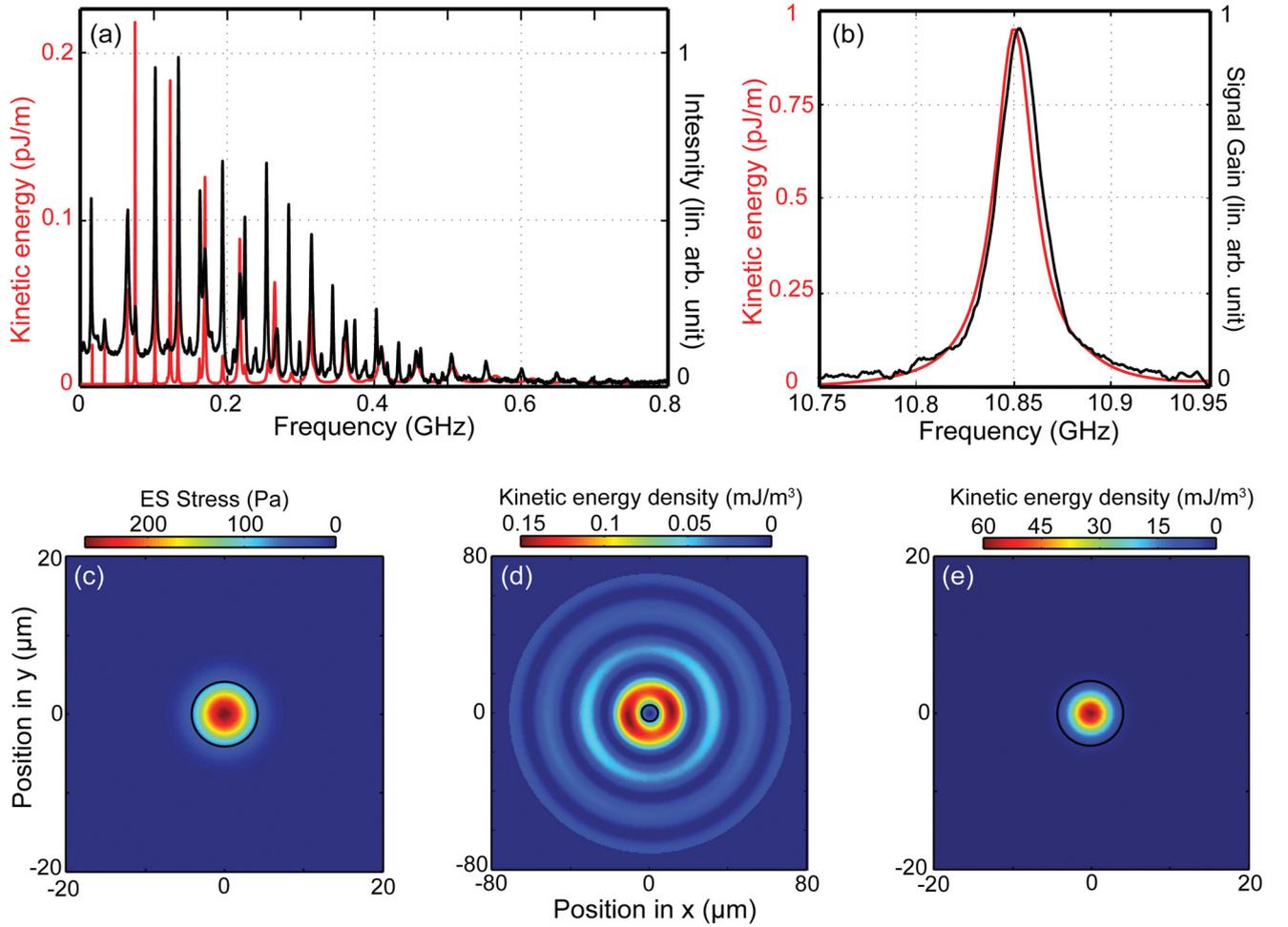
FIG. 1. (Color online) Comparison between experiment and ES model in single mode fiber (SMF28). (a) Experimental (black) and numerical (red) forward spectra ($k = 0$). (b) Experimental (black) and numerical (red) backward spectra ($k = 2k_1$). (c) Spatial distribution of the ES force generated by the fundamental optical mode at a wavelength of 1550 nm with 1 W optical power. The black circle limits the germanium doping core area. (d),(e) Computed kinetic energy density at 178 MHz (forward ES) and 10.85 GHz (backward ES).

diverge to infinity at resonance. Writing $\omega_n = \omega_{rn} + \iota\omega_{in}$,

$$U(\omega = \omega_{rn}) \approx \frac{\omega_{rn}}{2\iota\omega_{in}} \frac{U_n^\dagger X T^{(es)}}{U_n^\dagger K U_n} U_n. \qquad (7)$$

The first factor in this expression is proportional to the Q factor of the resonance. As the Q factor in our viscoelastic loss model scales with the inverse of frequency, it is clear that resonance peaks must decrease with increasing frequency, as observed experimentally and with the direct computation in the forward ES case.

Now it is clear that the above normal mode argument cannot explain observations for backward ES ($k = 2k_1$). Actually, as k becomes large, there exist more and more normal modes

within any frequency interval, and the above analysis in terms of a discrete spectrum of modes becomes inadequate. The backward case can instead be treated under the following short-wavelength approximation. For an optical wavelength of 1.55 μm in a vacuum, indeed, the optical wavelength in silica is about 1 μm and the acoustic phonon wavelength is thus about 500 nm. This is typically much smaller than the diameter of a classical optical fiber, but still comparable to the size of the core of some PCF or integrated optical waveguides. We consider specifically core diameters exceeding a few microns in the following discussion. Neglecting K_0 and kK_1 in the stiffness matrix expression, we have

$$k^2 K_2 U_B = \omega_B^2 M U_B, \qquad (8)$$

TABLE I. Independent material constants for isotropic silica (Ref. 14). Values for 0.36%-GeO$_2$-doped silica given in parentheses are deduced from (Ref. 15).

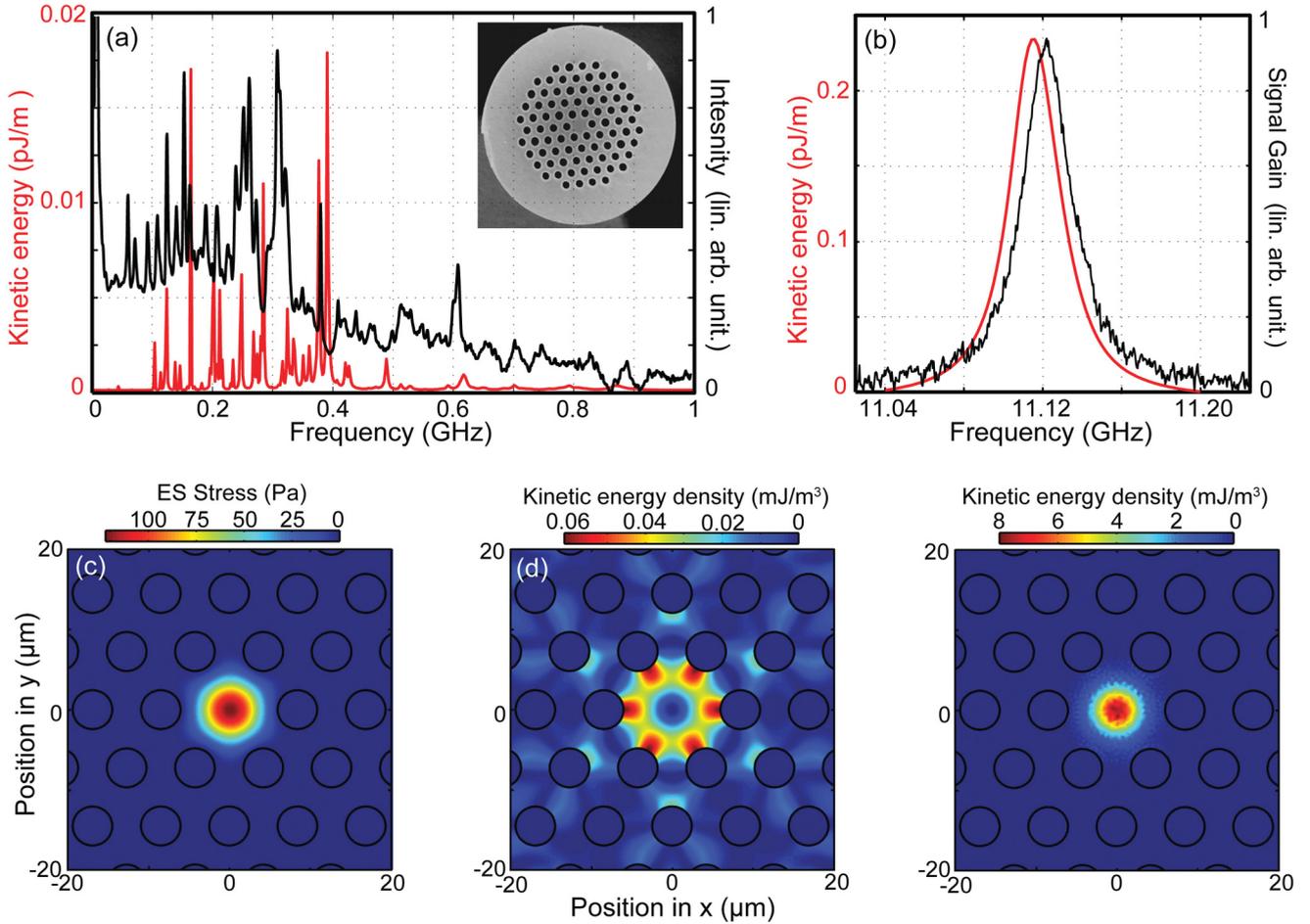|			
Elast. const., GPa	$c_{11} = 78$ (76)	$c_{12} = 16$ (16.15)	$c_{44} = 31$ (29.9)
Photoelast. const.	$p_{11} = 0.12$	$p_{12} = 0.27$	$p_{44} = -0.073$
Mat. dens., kg/m^3	$\rho = 2203$ (2254)		
Refractive index	$n = 1.444$ (1.4492) at $\lambda = 1550$ nm		

FIG. 2. (Color online) Comparison between experiment and ES model in large core PCF. (a) Experimental (black) and numerical (red) forward spectra ($k = 0$). The inset in (a) shows a cross-section of the fiber. (b) Experimental (black) and numerical (red) backward spectra ($k = 2k_1$). (c) Spatial distribution of the ES force generated by the fundamental optical mode at a wavelength of 1550 nm with 1 W optical power. (d),(e) Computed kinetic energy density at 390 MHz (forward ES) and 11.01 GHz (backward ES).

which defines the usual Brillouin frequency ω_B. U_B, the eigenvector corresponding to eigenfrequency ω_B, is a simple plane wave.[19] In the short-wavelength approximation, $X \approx kX_1$ and the electrostrictive force is mostly longitudinal because of the particular symmetries of the elasto-optic tensor of silica. As a consequence, shear waves satisfying Eq. (8) will hardly be excited and we can take U_B as dominantly longitudinally polarized, and the velocity ω_B/k_B as very close to the velocity for longitudinal waves in silica $\sqrt{c_{11}/\rho} = 5950$ m/s. It must be stressed that this situation is peculiar to silica, and would not necessarily apply to other materials, such as silicon. We further observe that because silica is isotropic, the solution to Eq. (8) is actually independent of the propagation direction. The actual response of the medium to the ES stress U can then be decomposed as an angular spectrum of plane waves, satisfying $k^2 K_2 U = \omega_B^2 M U$ to a good approximation for $\omega \approx \omega_B$. Replacing this relation in Eq. (5), we obtain that

$$U \approx \left[K_0 + k_B K_1 + \left(\omega_B^2 - \omega^2 \right) M \right]^{-1} X T^{\mathrm{es}}. \quad (9)$$

This expression represents a Lorentzian distribution centered on the Brillouin frequency. Close to resonance, the matrix to be inverted is of minimum norm, but nonvanishing because of phonon loss. Significantly, the transverse distribution of the phonon beam is similar to the electrostrictive stress distribution, T^{es}. This is very different from the forward case, for which this distribution is given by the normal modes of the fiber, and thus extends throughout the fiber cross section. Figure 3 illustrates this point by showing the profiles of the distribution of phonon energy. We believe this particular distribution of the phonon beam explains why SBS is remarkably efficient in optical fibers, independently of the fact that the involved acoustic phonons are guided or not by the transversal structure of the fiber. We note that the mechanism of guidance by the electrostrictive stress distribution relies on the incident optical waves being guided in the core of the fiber, and would not hold for SBS in bulk crystals, for example. A formal analogy can further be drawn with optical gain guidance in the plane of the junction of double-heterostructure semiconductor lasers.[20] But while confinement normal to the laser junction is provided mainly by the structural refractive index distribution and not by gain, electrostrictive stress is here solely responsible for guidance of the phonon beam.

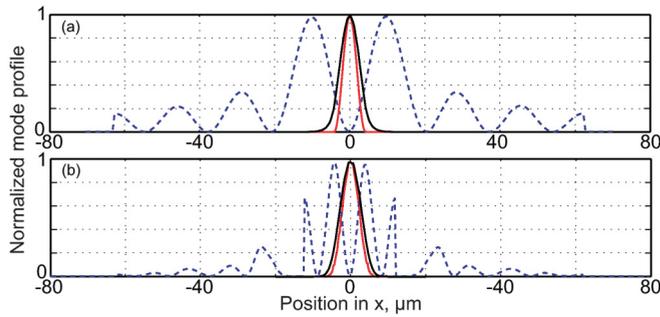It may be argued that if absorption would dominate over diffractive spreading of the phonon beam, then the new

FIG. 3. (Color online) Normalized *X* profiles of optical power density and kinetic energy density in (a) photonic crystal fiber and (b) standard fiber. The black line shows the fundamental optical mode guided by total internal reflection. The dashed blue line shows the most efficient elastic mode in the forward ES case and the red line shows the phonon beam excited in the backward ES case.

FIG. 4. (Color online) Computed backward ES spectrum and kinetic energy density at resonance for fiber SMF28, for a *Q* factor at resonance artificially increased 100-fold as compared to the experimental value.

phonons created all along the fiber core would not travel far before being absorbed, thus explaining the apparent phonon guidance described above. Let us show that this argument does not hold and that lower loss, strikingly, leads to the generation of a phonon beam that is even more confined to the core. The quality factor of the SBS resonance in SMF28 is about 450 and the longitudinal phonon wavelength is thus 540 nm. Phonons thus propagate over a distance of approximately 250 μm before getting absorbed. This distance is clearly much larger than the phonon beam spread observed in Fig. 3, which is about 8 μm. It is also larger than the fiber diameter. Let us artificially increase the *Q* factor of the resonance by a factor of 100, or correspondingly allow phonons to propagate over distances as large as 25 mm. Figure 4 shows the backward ES spectrum and the kinetic energy density at resonance computed in this case for fiber SMF28. The spectrum is 100 times less wide, as expected, and the phonon energy distribution is even more confined to the core as compared to the case of Fig. 1(e). Clearly, phonon guidance is not a result of phonon loss in the frame of our model, but rather results from the spatial distribution of the optical force.

As a conclusion, the consideration of electrostrictive forces has allowed us to evaluate precisely the acoustic phonons generat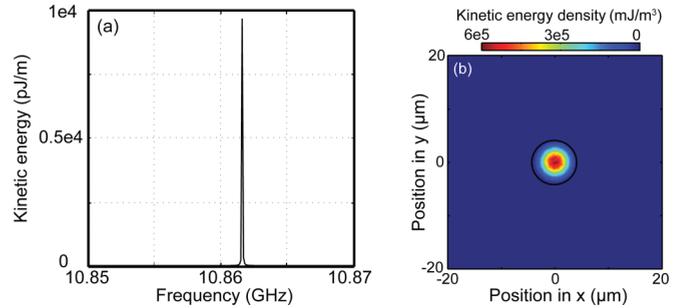ed in optical fibers by Brillouin-type interactions. Our model encompasses the forward interaction case, including GAWBS, and the backward interaction case, including SBS. In all expressions we have derived, the frequency response to electrostriction is a Lorentzian function whose width is dictated by intrinsic phonon losses, or the inverse of the phonon life time, possibly dependent on frequency. Significantly, the phonon beam generated via backward ES is naturally guided and confined to the core of the fiber. Our method could furthermore be extended to almost any type of optical waveguide. Silicon nanostructures, for instance, have attracted attention recently in view of obtaining optomechanical coupling in structures supporting the simultaneous confinement of elastic and optical waves.[21] Optical forces, including ES and radiation pressure,[22] have been predicted to scale to large values in nanoscale waveguides.[3] The model we have presented, possibly supplemented with optical surface force terms, should yield the acoustic phonons generated in such cases.

ACKNOWLEDGMENTS

*vincent.laude@femto-st.fr

[1]R. W. Boyd, *Nonlinear Optics*, 3rd ed. (Academic, New York, 2008).

[2]M. S. Kang, A. Brenn, and P. St. J. Russell, Phys. Rev. Lett. **105**, 153901 (2010).

[3]P. T. Rakich, C. Reinke, R. Camacho, P. Davids, and Z. Wang, Phys. Rev. X **2**, 011008 (2012).

[4]M. S. Kang, A. Nazarkin, A. Brenn, and P. St. J. Russell, Nat. Phys. **5**, 276 (2009).

[5]D. Elser, U. L. Andersen, A. Korn, O. Glöckl, S. Lorenz, C. Marquardt, and G. Leuchs, Phys. Rev. Lett. **97**, 133901 (2006).

[6]R. M. Shelby, M. D. Levenson, and P. W. Bayer, Phys. Rev. B **31**, 5244 (1985).

[7]P. Dainese, P. St. J. Russell, N. Joly, J. Knight, G. Wiederhecker, H. Fragnito, V. Laude, and A. Khelif, Nat. Phys. **2**, 388 (2006).

[8]J.-C. Beugnot, T. Sylvestre, H. Maillotte, G. Mélin, and V. Laude, Opt. Lett. **32**, 17 (2007).

[9]Y. R. Shen and N. Bloembergen, Phys. Rev. **137**, A 1787 (1965).

[10]N. M. Kroll, J. Appl. Phys. **36**, 34 (1965).

[11]V. Laude, A. Khelif, S. Benchabane, M. Wilm, T. Sylvestre, B. Kibler, A. Mussot, J. M. Dudley, and H. Maillotte, Phys. Rev. B **71**, 045107 (2005).

[12]J. C. Beugnot, T. Sylvestre, D. Alasia, H. Maillotte, V. Laude, A. Monteville, L. Provino, N. Traynor, S. F. Mafang, and L. Thévenaz, Opt. Express **15**, 15517 (2007).

[13]R. P. Moiseyenko and V. Laude, Phys. Rev. B **83**, 064301 (2011).

[14] D. Royer and E. Dieulesaint, *Elastic Waves in Solids* (Wiley, New York, 1999).

[15] Y. Koyamada, S. Sato, S. Nakamura, H. Sotobayashi, and W. Chujo, J. Lightwave Technol. **22**, 631 (2004).

[16] P. J. Thomas, N. L. Rowell, H. M. van Driel, and G. I. Stegeman, Phys. Rev. B **19**, 4986 (1979).

[17] P. Dainese, P. St. J. Russell, G. S. Wiederhecker, N. Joly, H. L. Fragnito, V. Laude, and A. Khelif, Opt. Express **14**, 4141 (2006).

[18] G. S. Wiederhecker, A. Brenn, H. L. Fragnito, and P. St. J. Russell, Phys. Rev. Lett. **100**, 203903 (2008).

[19] The eigenvector is actually exactly a plane wave if the material constituting the waveguide is homogeneous, in which case Eq. (8) is simply the Cristofell equation for elastic waves in solids.

[20] D. D. Cook and F. R. Nash, J. Appl. Phys. **46**, 1660 (1975).

[21] D. Van Thourhout and J. Roels, Nature Photonics **4**, 211 (2010).

[22] T. Kippenberg and K. Vahala, Science **321**, 1172 (2008).